Vertical Structure of Horizontal Velocity in Regular Shoaling Waves: Comparisons with Boussinesq Theories

by

Chandrasekher Narayanan and John D. McCaplin

RESEARCH REPORT NO. CACR-95-08
June, 1995

CENTER FOR APPLIED COASTAL RESEARCH

Ocean Engineering Laboratory
University of Delaware
Newark, Delaware 19716

Vertical Structure of Horizontal Velocity in Regular Shoaling Waves: Comparisons with Boussinesq Theories

Chandrasekher Narayanan
and
John D. McCalpin
College of Marine Studies
and
Center for Applied Coastal Research
University of Delaware

June 7, 1995

Abstract

We investigate the parameterization of the vertical structure of horizontal velocity in a family of weakly nonlinear, weakly dispersive (Boussinesq) models developed by Nwogu. That model contains a free parameter which specifies the depth about which the assumed quadratic velocity profiles are expanded, with most standard formulations recovered by particular choices of this free parameter. Nwogu chose to optimize this model by selecting the parameter to best fit the linear dispersion relation. Here we test the model by applying it to the nonlinear case of shoaling of regular (cnoidal) waves. A new dataset documenting the vertical dependence of horizontal velocity is presented and is used to evaluate the range of values of the free parameter for which the model gives good results. We show that the Boussinesq model optimized for the best linear dispersion relation also gives the best approximation to the local vertical structure in this strongly nonlinear case.

1 Introduction

Much of the current research on the evolution of surface gravity waves in the nearshore environment is based on models of the Boussinesq type. These models assume low-order expansions of the dependent variables in the vertical direction, and by use of the

assumptions of weak nonlinearity and weak dispersiveness, are able to parameterize the variation of the flow field in the vertical direction in terms of purely horizontal measures. This reduction of a three-dimensional problem to a two-dimensional problem provides the computational efficiency which has been an important factor in the success of the approach.

The Boussinesq equations that are now considered to be the "standard" form are due to Peregrine [5]. These equations were obtained by integrating the Euler equations over the depth of the fluid and assuming weak nonlinearity and weak dispersiveness. The equations are able to describe the nonlinear refraction and diffraction of irregular, multi-dimensional waves in shallow water. Madsen and Mei [2] obtained the same set of equations by using perturbation expansions. There are various forms of the Boussinesq equations, all having lower order polynomial expansions in the vertical direction, and differing primarily in the selection of the dependent variables. McCowan [3] describes the practical range of the various forms of the Boussinesq equations. Nwogu [4] derived an alternative form of the equations using velocity at an arbitrary distance from the still water level as the velocity variable. By selection of specific values of the relative depth about which to make the polynomial expansion, one can recover most of the previously investigated forms of the equations. For the "best" choice of the expansion depth, these equations have excellent linear dispersion characteristics and are applicable for waves propagating in relatively deep water.

In this work, we document the parameterization of Nwogu's Boussinesq model for the vertical structure of horizontal velocity in regular (cnoidal) shoaling waves, as a function of the free parameter. These predictions are then compared with a new dataset of measured values from our laboratory. We discuss the evolution of the velocity field across the shoaling region, and its implications for the perturbation expansions employed by all Boussinesq models.

2 The Boussinesq Model

The Boussinesq models are long-wave models, based on perturbations of the shallow water equations. A simultaneous expansion in small nonlinearity (ϵ = wave amplitude / depth) and small dispersion (μ^2 = (depth/horizontal scale)^2) is performed. If ϵ and μ^2 are not of the same order, further simplifications are possible, leading to the linear long-wave and Airy theory at the two extremes. Boussinesq models are characterized by the assumption that ϵ and μ^2 are both small and of the same order. They share this assumption with the KdV and regularized long-wave theories, but generalize these theories by not assuming unidirectional propagation.

The Boussinesq model investigated here is the formulation of Nwogu [4]. Nwogu chooses an arbitrary relative depth ($\alpha \equiv z_\alpha/h$, where h is the local still-water thickness of the fluid) about which to perform the series expansions of the vertical structure of

the dependent variables. The dependent variables of the 2-D model are then assumed to be equal to the values of the 3-D solution at that relative depth, and are denoted with a subscript α. The vertical variation of the vertical velocity is assumed to be linear, consequently the vertical variation of the horizontal velocity components is assumed to quadratic. The reader is referred to [4] for the derivation of the equations.

For application to wave shoaling in a narrow wave tank, we may assume the flow to be one-dimensional, for which the equations reduce to

$$\eta_t + [(h+\eta)u_\alpha]_x + \left[(\frac{z_\alpha^2}{2} - \frac{h^2}{6})hu_{\alpha xx} + (z_\alpha + \frac{h}{2})h(hu_\alpha)_{xx}\right]_x = 0 \tag{1}$$

$$u_{\alpha t} + g\eta_x + u_\alpha u_{\alpha x} + \left[\frac{z_\alpha^2}{2}u_{\alpha xt} + z_\alpha(hu_{\alpha t})_x\right]_x = 0. \tag{2}$$

These equations are in dimensional form and accurate to $O(\epsilon, \mu^2)$, and hence allow weak nonlinearity and weak dispersion.

The expression for the horizontal velocities as a function of z is

$$u = u_\alpha + \left(\frac{z_\alpha^2}{2} - \frac{z^2}{2}\right)u_{\alpha xx} + (z_\alpha - z)(hu_\alpha)_{xx}. \tag{3}$$

The free parameter of the model is $\alpha = z_\alpha/h$. In the following, it is more convenient to use

$$\tilde{\alpha} = \frac{1}{2}\left(\frac{z_\alpha}{h}\right)^2 + \frac{z_\alpha}{h}, \tag{4}$$

which can be chosen to select the different forms of Boussinesq equations, as discussed below.

The dispersion relation of the linear one-dimensional model is

$$C^2 = \frac{\omega^2}{k^2} = gh\left[\frac{1 - (\tilde{\alpha} + \frac{1}{3})(kh)^2}{1 - \tilde{\alpha}(kh)^2}\right] \tag{5}$$

where C is the phase speed, ω the frequency, k the wavenumber, and where $\tilde{\alpha}$ is defined above.

Four choices of the free parameter were chosen for comparison with the laboratory data

- Depth-averaged

$$\tilde{\alpha} = -\frac{1}{3} \tag{6}$$

$$\frac{z_\alpha}{h} = \left(-1 + \frac{1}{\sqrt{3}}\right) \approx -0.423 \tag{7}$$

This corresponds to the depth-averaged case derived by Peregrine [5], and is the mostly commonly utilized form of the equations. The dispersion relation for this case is

$$C^2 = gh\left[\frac{1}{1 + \frac{1}{3}(kh)^2}\right]. \tag{8}$$

- Still-water

$$\tilde{\alpha} = 0 \tag{9}$$

$$\frac{z_\alpha}{h} = 0 \tag{10}$$

This results from the expansion of the vertical structure about the values at the still-water level. The dispersion relation is

$$C^2 = gh\left[1 - \frac{1}{3}(kh)^2\right]. \tag{11}$$

- Bottom

$$\tilde{\alpha} = -\frac{1}{2} \tag{12}$$

$$\frac{z_\alpha}{h} = -1 \tag{13}$$

This results from the expansion of the variables about the values at the bottom. The dispersion relation is

$$C^2 = gh\left[\frac{1 + \frac{1}{6}(kh)^2}{1 + \frac{1}{2}(kh)^2}\right]. \tag{14}$$

- Best-linear-fit

$$\tilde{\alpha} \approx -0.390 \tag{15}$$

$$\frac{z_\alpha}{h} \approx -0.53 \tag{16}$$

This is the value derived by Nwogu as providing the best fit to the exact linear dispersion relation of Airy theory, as discussed below. The dispersion relation is best understood by its graphical representation in Fig. 1.

The phase speeds resulting from these four choices of $\tilde{\alpha}$ are presented in Fig. 1, along with the exact dispersion relation from Airy theory:

$$C^2 = gh\frac{\tanh kh}{kh} \tag{17}$$

3 Laboratory Experiments

3.1 Configuration

The experiments for this project were conducted at the Ocean Engineering Laboratory, University of Delaware. The laboratory houses a precision wave tank (33 m long with

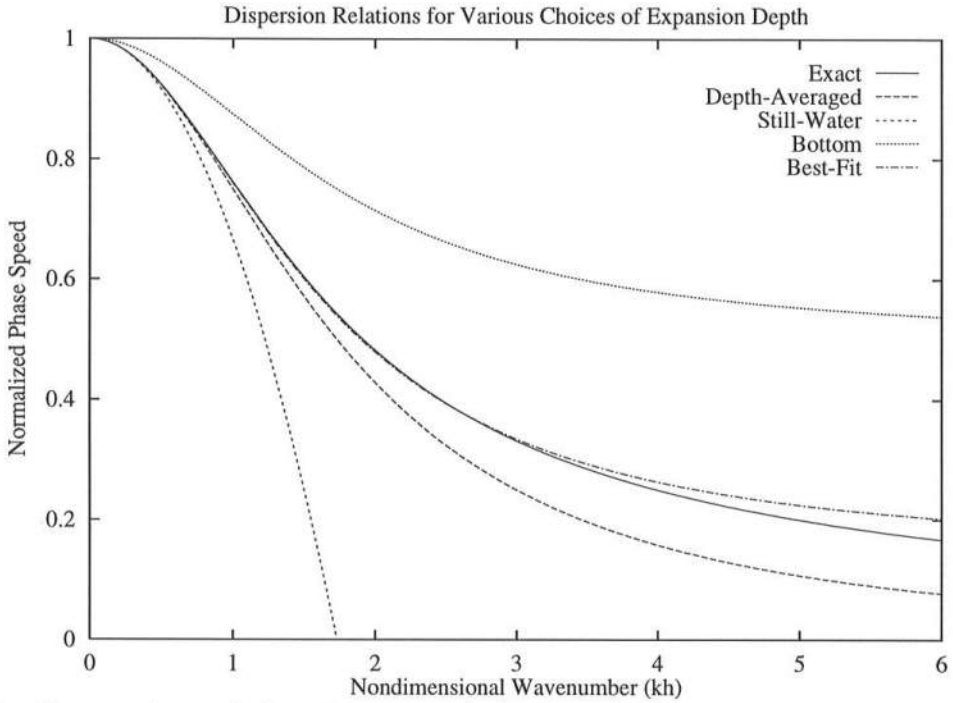

Figure 1: Comparison of the phase speeds for various forms of the Boussinesq equations relative to the Airy theory.

0.6 m by 0.76 m cross-section). Waves were generated by a hydraulically actuated wave maker at one end of the tank. The wavemaker is capable of creating sinusoidal, cnoidal and solitary waves, as well as random sea state. A moving instrument mounted on the rail facilitates measuring waves along the length of the tank. An adjustable beach is installed at the far end of the tank. A corion false bottom was installed to create the slope. An IBM PS/2 model 30 286 computer was used to send impulses to the wavemaker and a feedback system consisting of a linear variable differential transformer was used to minimize the difference between the desired position of the wave plate and the actual position. The control signal for the wave generator was developed using the numerical scheme by Goring [1].

A Dantec fiber optic laser system, powered by a 4 W argon-ion Lexel laser was used to measure the horizontal component of velocity. This Laser Doppler Anemometer (LDA) is a backscatter, four-beam laser system, with a transmitter and frequency tracker. The fiber optic laser probe used was 14 mm with focal length of 50 mm and beam spacing of 8 mm.

The water surface elevation was measured using capacitance wave gauges mounted on an instrument carriage along the top of the tank on two rails.

A second IBM PS/2 model 30 286 installed with a MetraByte DASH-16F data acquisition board was used to collect the data using the STREAMER software. The two computers were linked so that all the data could be taken by one computer.

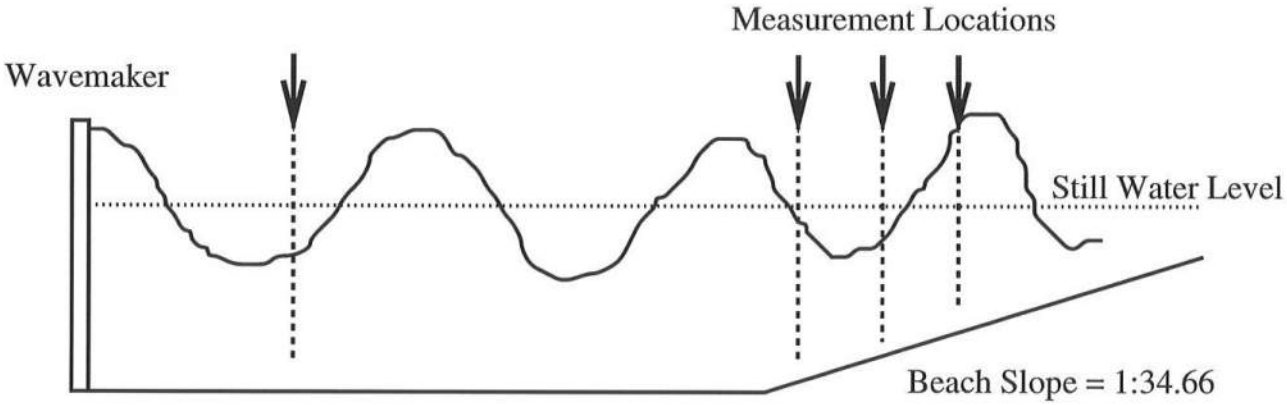

Figure 2: The experimental set-up (not to scale). At each measuring location measurements were made of wave height and of wave velocity at 7–11 levels in the vertical.

Parameter	Station 1	Station 2	Station 3	Station 4
x (m)	-2.19	6.58	7.19	7.44
h (cm)	40.0	21.0	19.2	18.5
η_{max} (cm)	9.7	13.0	13.8	14.5
η_{min} (cm)	−2.4	−3.0	−2.9	−3.0

Table 1: Beach geometry and Wave amplitude parameters at the measuring stations. x is the distance in m from the toe of the beach, h is the still-water depth in cm at each station, and η is the deviation in cm from the still-water depth.

Because the LDA is a single-point measuring device, we required a highly repeatable waveform for the generation of our vertical profiles. Although solitary waves would have been ideal, the waiting time between measurements (for the water in the wave tank to become calm) was prohibitive. We have had excellent success with the repeatability of cnoidal waves after an initial spin-up period, and these were used for all the experiments discussed here.

Two different wave conditions, a plunging breaker of period 5 s and a spilling breaker of period 2 s, were chosen. Four different positions (stations) along the length of the tank were chosen to make measurements for each of the above conditions. The first position was in the flat bottom region and the other three positions were along the slope in the shoaling (pre-breaking) region. At each of these four stations, between 7 and 11 positions were chosen in the vertical where velocity measurements were taken. The parameters are presented in Table 1.

The slope of the tank was held constant at 1:34.66 for all the experiments. The distance from the wavemaker to the slope was 11.85 m. The still water depth in the constant-depth region of the wave tank was 0.4 m for all the experiments. The Doppler frequency range used was 33 to 333 KHz for all cases. The wave height, for all waves, was 0.12 m. In the case of plunging breaker, data were collected at a sampling rate of 128 Hz and for the case of the spilling breaker, the sampling rate was 256 Hz. In both the cases approximately 50 waves were collected for each point, and the results were ensemble-averaged. The cnoidal waves were allowed half an hour to stabilize before data were taken. This ensured a steady-state condition in the wave tank.

The velocity measurements were conducted using the 8 mm probe, which was placed on a stand so that it could be moved vertically. The crossing point of the beams was several centimeters into the wave tank. The wall effects did not interfere with the measurements because the measurements were taken outside the lateral boundary layer.

3.2 Summary of Data

We generated a cnoidal wave that resulted in a spilling breaker by choosing a 2 s period and a flat-bottom amplitude of 0.12 m. A wave resulting in a plunging breaker was generated by choosing a 5 s period with the same 0.12 m amplitude. The evolution of the wave height for the two cases is shown in Fig. 3.

The raw data (both height and horizontal velocity) for the 2 s wave consisted of time series for 132 s (corresponding to 66 waves), while the total sampling time for the 5 s wave was 265 s (corresponding to 53 wave periods).

For analysis, the data was ensemble-averaged and low-pass filtered (with a 10 Hz cutoff). To demonstrate the data reproducibility, a sample raw data set superimposed on the ensemble averaged, low-pass filtered horizontal velocity is shown in Fig. 4.

The data at each depth were aligned by matching the peaks of the water surface elevation. An example of the ensemble-averaged horizontal velocity is shown at the different depths (figure 5). We calculated the maximum and minimum velocities of the ensemble-averaged data and fit cubic polynomial curves to these data using the least-squares method. To improve the behavior of the fitted curves near the bottom, we forced the curves to have no vertical derivative at the bottom. This is approximately consistent with a no stress boundary condition at the bottom. Since the bottom is not exactly flat, this is not exact — "no stress" implies no normal derivative instead of no vertical derivative — but the error is negligible for the 1:34.66 slope geometry used here.

The least-squares fit provides the coefficients for analytical expressions for $u(z)$ for each measuring location and wave type. The equation is of the form

$$\frac{u(z)}{\sqrt{gh}} = a\left(\frac{z_\alpha}{h}\right)^3 + b\left(\frac{z_\alpha}{h}\right)^2 + c\left(\frac{z_\alpha}{h}\right) + d \tag{18}$$

Cubic polynomials were chosen to obtain from the data an indication of the change in

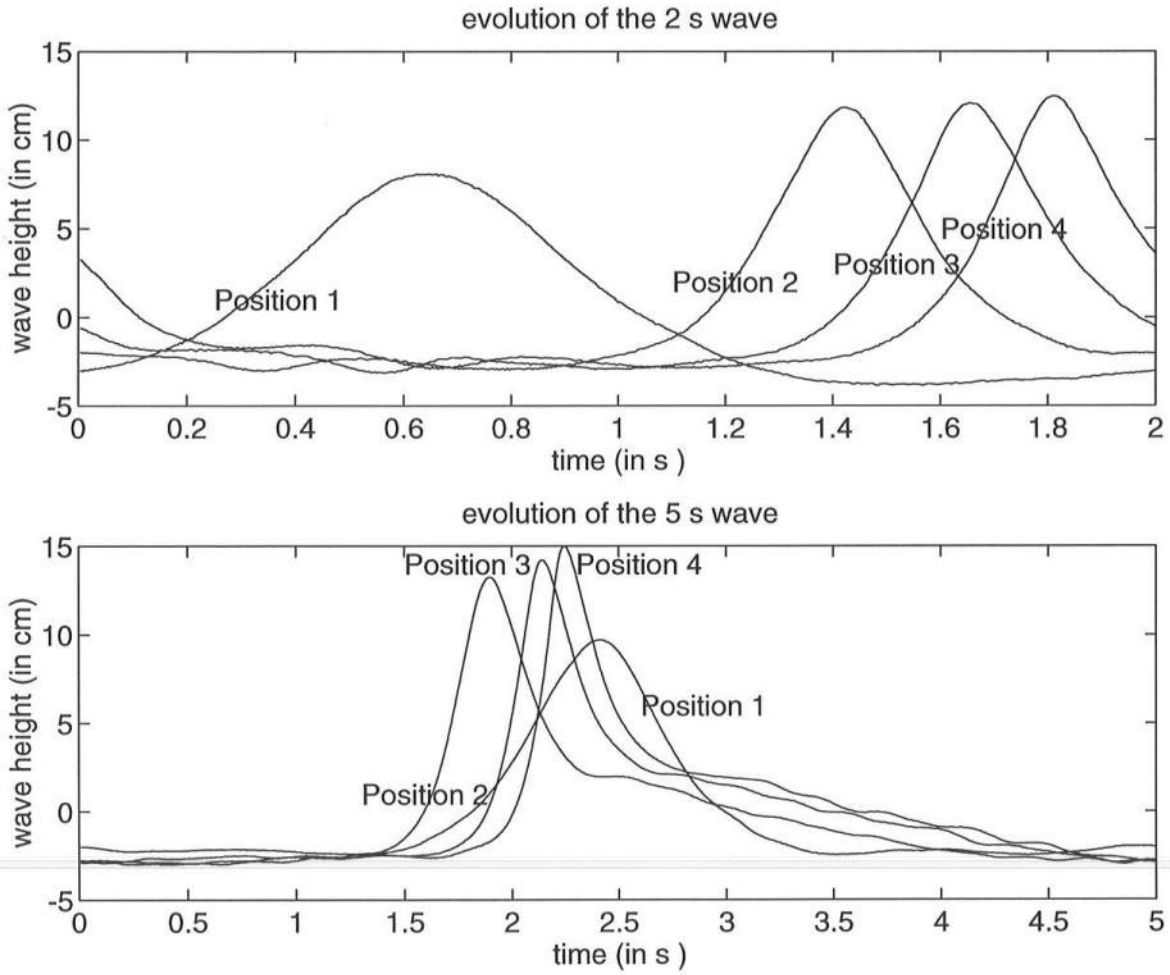

Figure 3: The evolution of the 2 s wave and 5 s wave

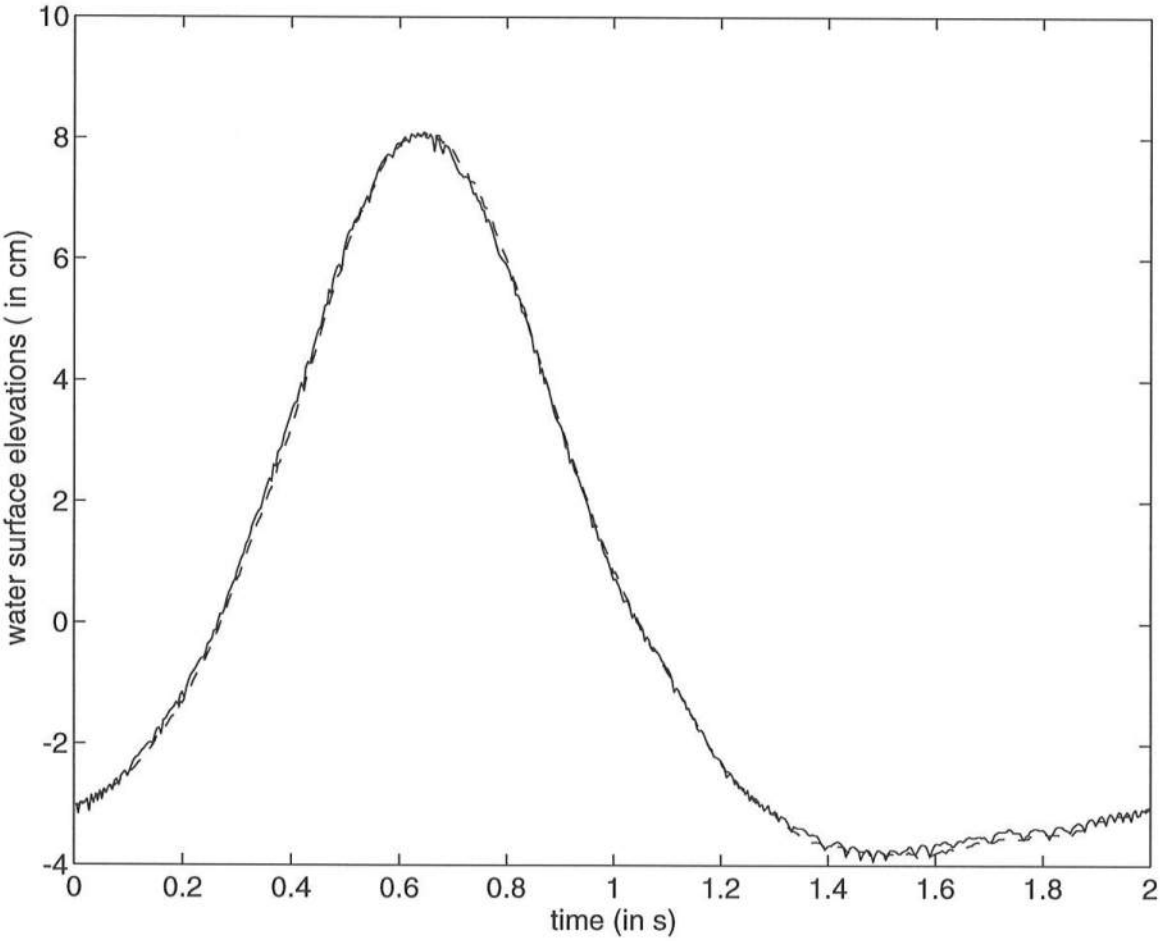

Figure 4: A sample raw data set superimposed on the ensemble-averaged data set. The period of this wave is 2 s. The dashed lines denote the ensemble-averaged data set and the solid line denotes the raw data.

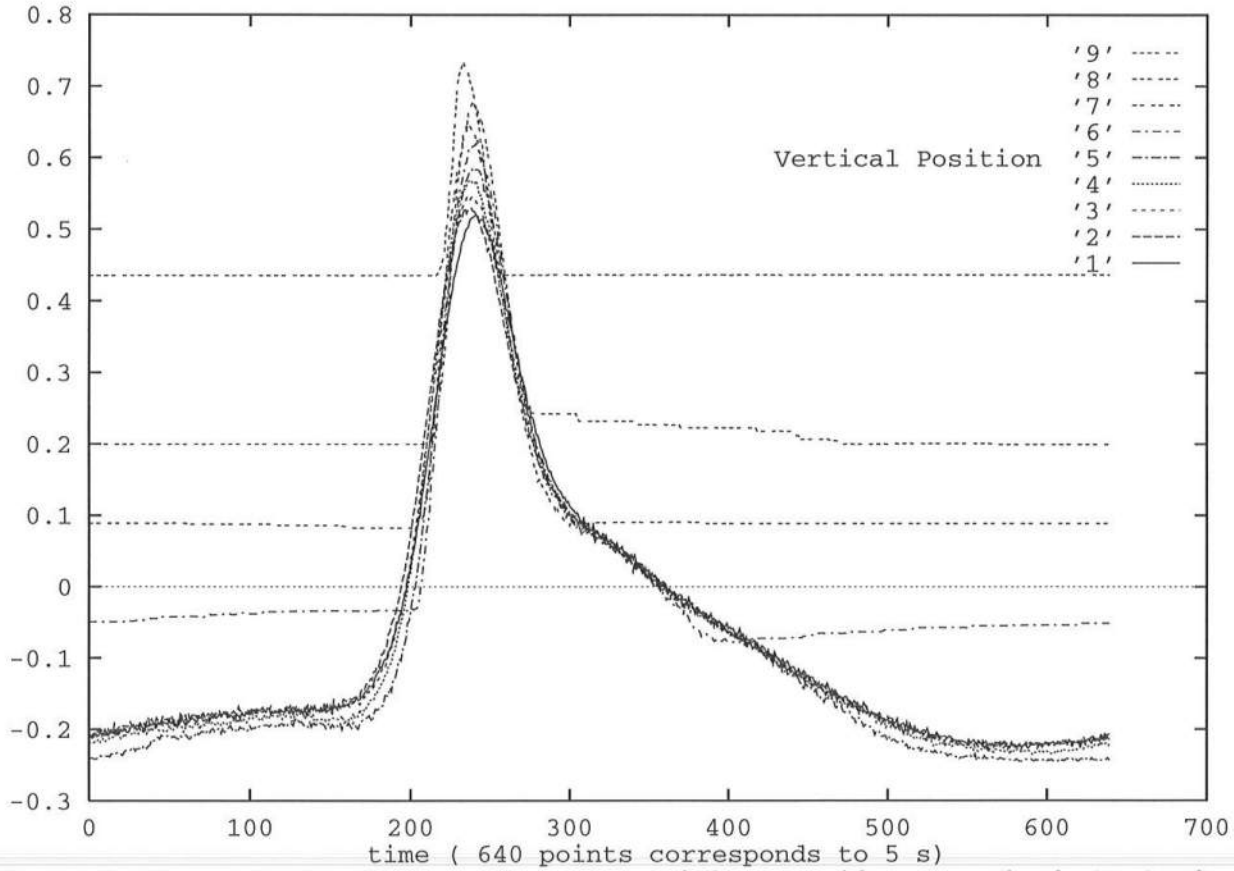

Figure 5: The vertical and temporal structure of the ensemble-averaged velocity in the shoaling region for a sample data set. Curve 1 is near the bottom, curve 9 is near the crest. Horizontal lines indicate that the measuring volume was out of the water during that portion of the wave cycle.

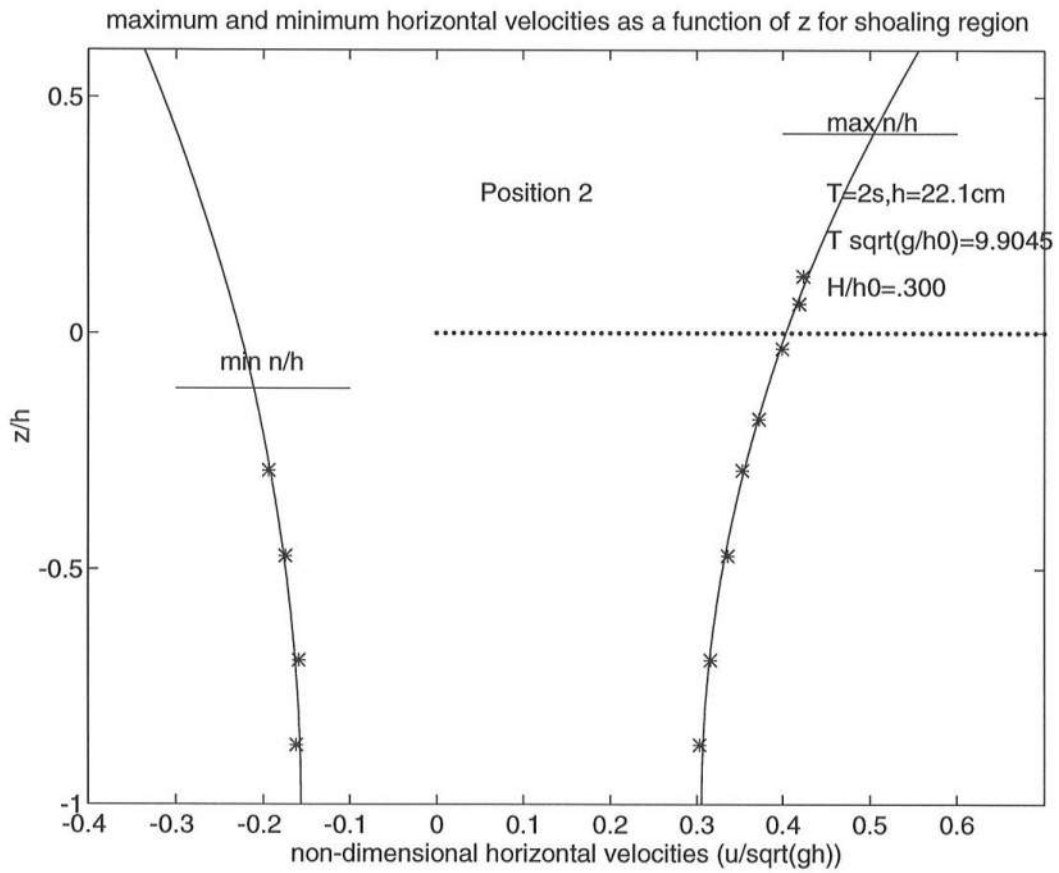

Figure 6: The vertical structure of the ensemble-averaged maximum and minimum velocities at station 2 in the shoaling region for the 2 s (spilling) wave.

z of u_{zz}. Quadratic curves also fit the data well, but correspond to exactly the same truncation as the Boussinesq model itself, and provide no indication of the errors in that model. This will be further discussed in the following section.

Observations were made up to near the top of the water column, but the data above the still water line were not used in the analysis. The poor quality of the data above the still water line was due to the loss of the leading and trailing edges of the signal when the water surface broke either of the laser beams, and the inability of the electronics to rapidly reaquire the signal after this disruption. The vertical structure of a typical ensemble-averaged dataset is presented in Figure 6, along with the cubic polynomial least squares fit. In this case, the LDA was unable to provide usable data in the top $\approx 15\%$ of the water column, but the remaining data is accurate for the bulk of the water column, and provides adequate resolution of the large-scale vertical distribution of horizontal velocity.

4 Discussion

As noted previously, the (generalized) Boussinesq approximation for $u(z)$ is given by

$$u = u_\alpha + \left(\frac{z_\alpha^2}{2} - \frac{z^2}{2}\right) u_{\alpha xx} + (z_\alpha - z)(hu_\alpha)_{xx}. \tag{19}$$

It is important to note that this equation does not contain the nonlinear parameter, ϵ, (nor does it enter at higher orders in the expansion, which is strictly in terms of μ^2). This suggests that nonlinearity may not directly contribute to modification of the vertical structure of horizontal velocity, and therefore that adjusting the free parameter to optimize the kinematics of the linear problem is the correct approach even for problems with nonlinearity.

Evaluation of this function requires knowledge of both u_α and $u_{\alpha xx}$. For a given z_α, u_α was obtained from the fitted curves. The values of $u_{\alpha xx}$ are not available directly from the measured data and must be approximated. Since the flow fields are non-divergent and (before breaking) irrotational, the horizontal velocity obeys Laplace's equation, so that

$$u_{xx} = -u_{zz} \tag{20}$$

and the value of $u_{\alpha xx}$ can be obtained directly from the cubic expression for the vertical dependence. This makes it clear why a quadratic polynomial fit would be inappropriate here — the value of u_{zz} (and hence $u_{\alpha xx}$) would be independent of α. While the Boussinesq approximation would still show a dependence on α in that case, it would not be based on the correct local kinematics.

Using station 2 of the 2 s (spilling) case, Figure 7 shows the Boussinesq approximations of the vertical profile of horizontal velocity for several values of α. In order to make the small differences stand out more clearly for intermediate values of $\tilde{\alpha}$, the velocities scaled by the curve-fitted velocity at each depth are presented in Figure 8.

Under the crest of each wave, the RMS difference between the Boussinesq approximation of $u(z)$ and the fitted curve for $u(z)$ were computed as a function of $\tilde{\alpha}$ (using 20 values of α to fill in the curves). The results for the 2 s (spilling) wave are presented in Figure 9 for the 5 s (plunging) wave are presented in Figure 10. Recall that station 1 is on the flat bottom, several m before the beginning of the bottom slope. For the 2 s wave, the nonlinearity and dispersion are approximately balanced at this location, while the 5 s wave has significantly more nonlinearity than dispersion. The two curves show a remarkably common structure, with minimal errors occurring between $\alpha = -0.33$ and $\alpha = -0.43$ in all cases — very close to Nwogu's "optimal" value of $\alpha = -0.39$ for the linear case. There is some indication that the optimal value of α increases slightly across the shoaling zone for the 2 s wave (from -0.39 to -0.43), but there is no evidence of such a shift in the results for the 5 s wave.

This result is a bit surprising, since it is not at all clear *a priori* that optimizing the linear dispersion relation would give the correct vertical structure of the horizontal

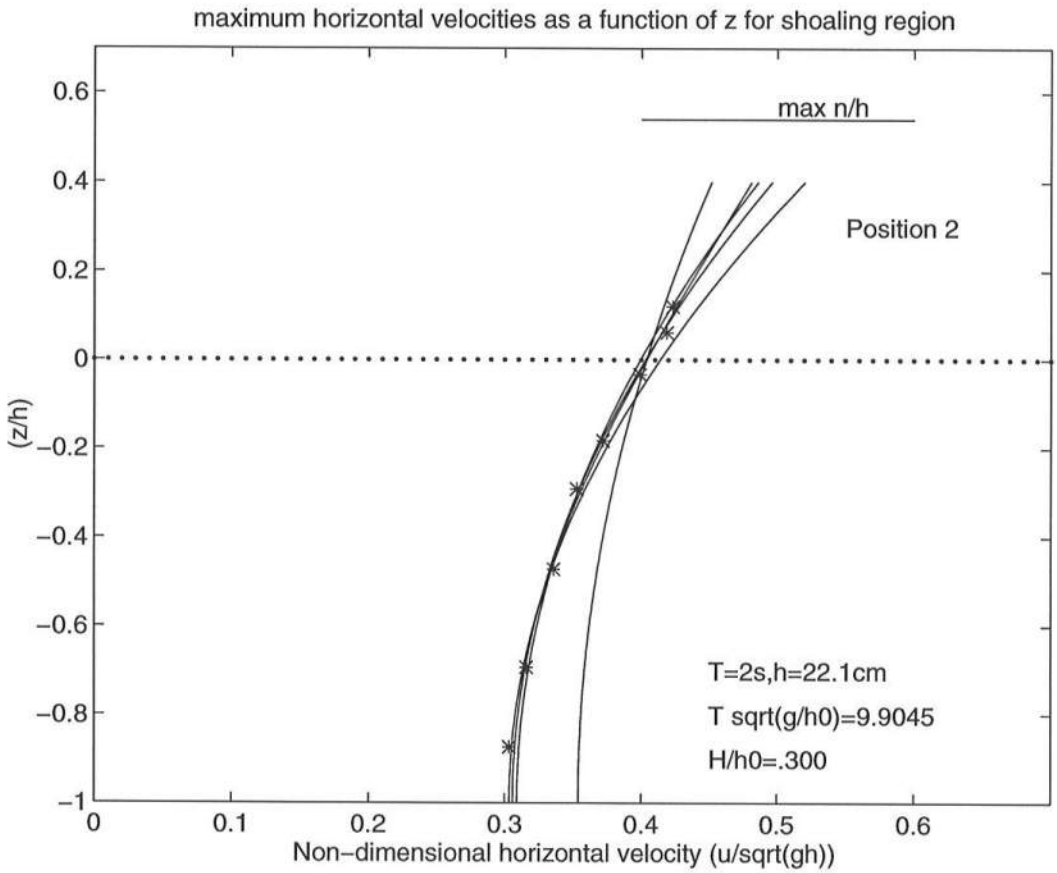

Figure 7: Several Boussinesq estimates of the vertical structure of horizontal velocity at station 2 in the shoaling region for the 2 s (spilling) wave. The curves are based on (across the top from left to right): still-water, cubic fit to data, depth-averaged, Nwogu, and bottom.

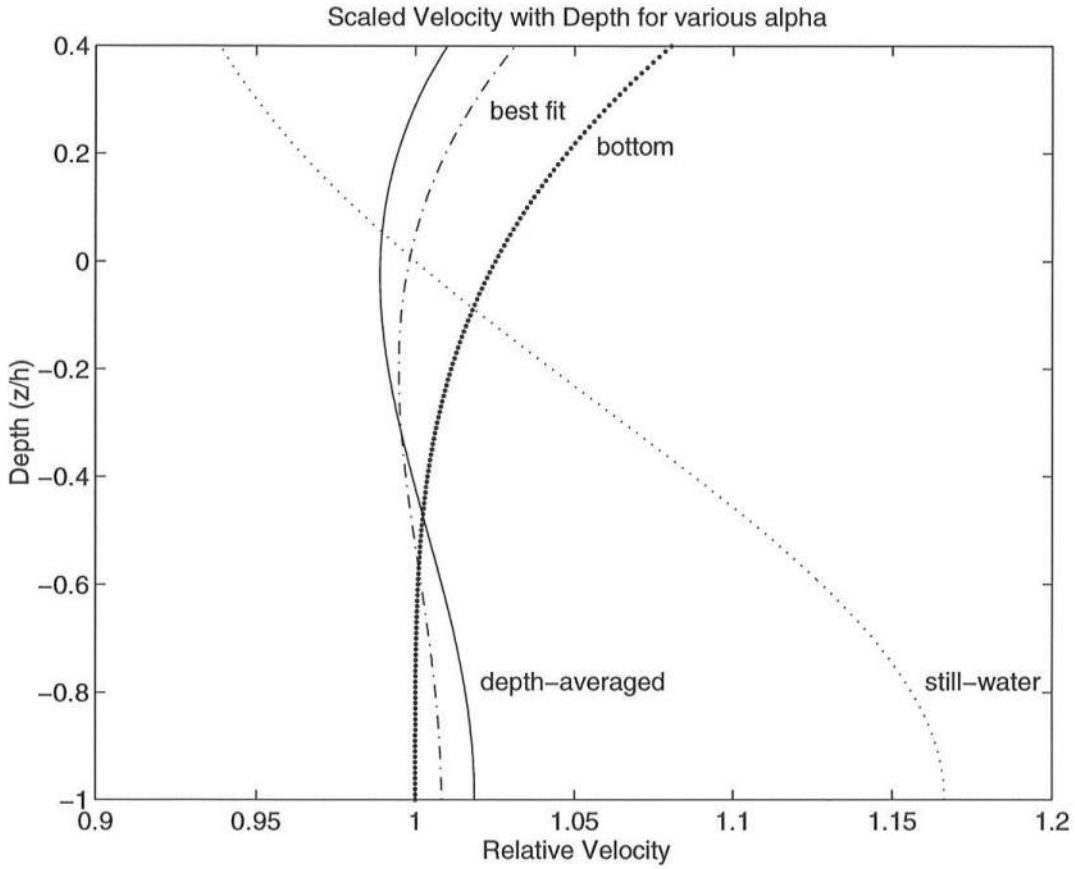

Figure 8: Velocities scaled by the curve-fitted velocity for several values of $\tilde{\alpha}$ for station 2 of the 2 s (spilling) wave. The solid curve is for the depth-averaged case ($\tilde{\alpha} = -1/3$); the dot-dash curve for Nwogu's best-fit case ($\tilde{\alpha} = -0.390$); the tightly dotted curve for the expansion about the bottom velocity ($\tilde{\alpha} = -1/2$; and the widely dotted curve for the expansion about the velocity at the still-water level ($\tilde{\alpha} = 0$).

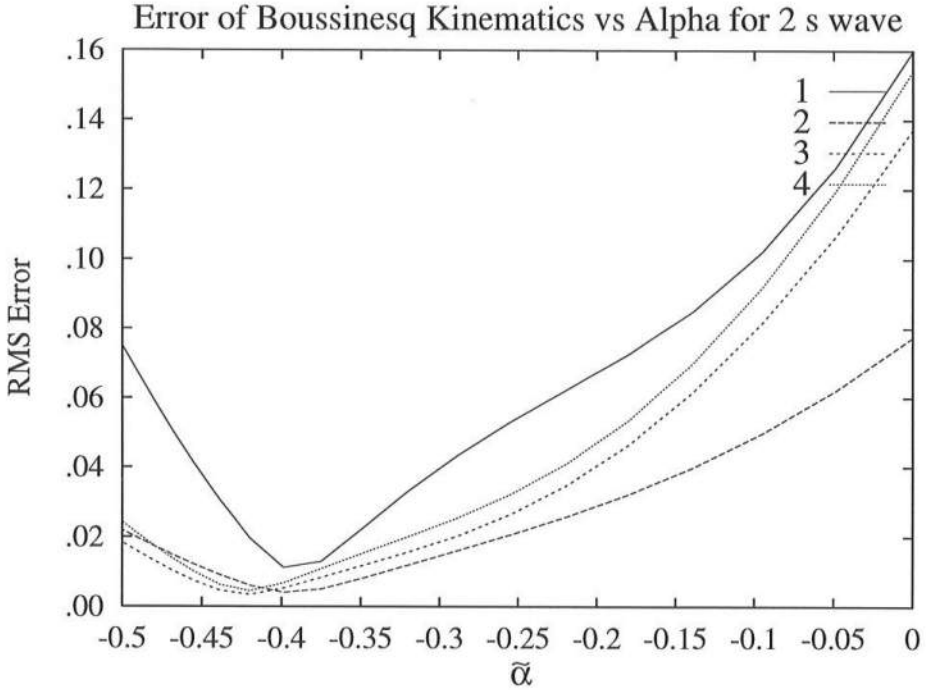

Figure 9: RMS error in fitting $u(z)$ as a function of $\tilde{\alpha}$ at stations 1–4 progressing through the shoaling zone for the 2-second (spilling) wave.

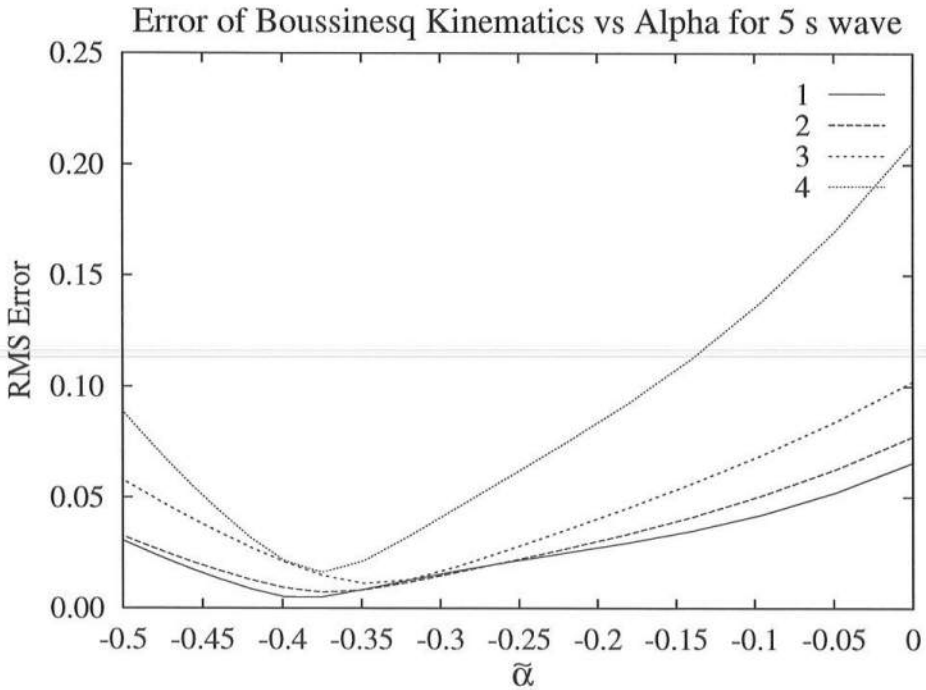

Figure 10: RMS error in fitting $u(z)$ as a function of $\tilde{\alpha}$ at stations 1–4 progressing through the shoaling zone for the 5-second (plunging) wave.

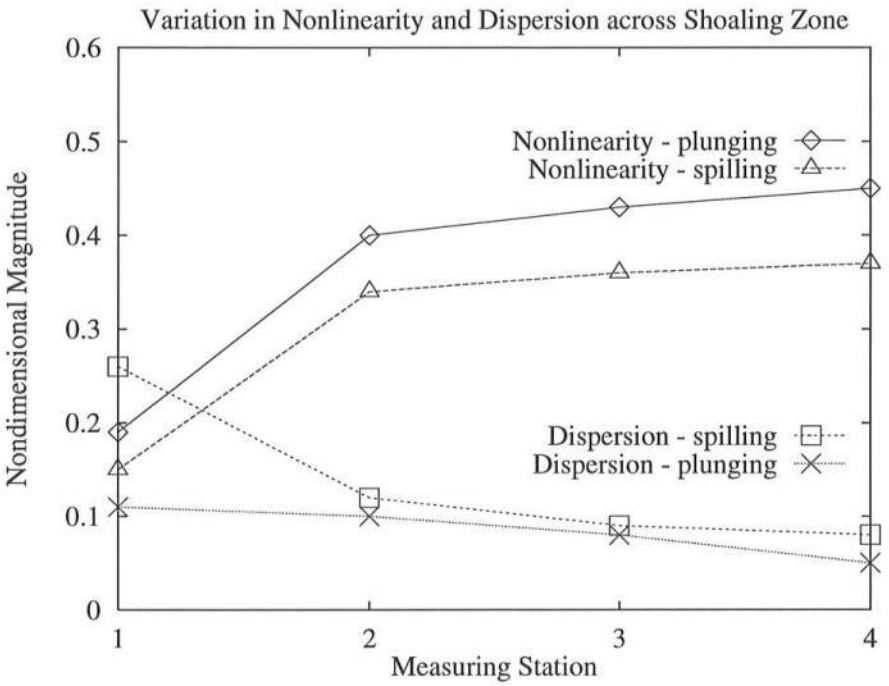

Figure 11: Estimates of the nonlinearity (ϵ) and dispersion (μ^2) as a function of position in the shoaling zone for the 2 s (spilling) and 5 s (plunging) waves. All values are defined under the wave crest.

velocity. The lack of explicit dependence on nonlinearity is less surprising, since the expression for the vertical structure of horizontal velocity does not depend on ϵ at any order. The result is also fortuitous, since it means that we do not need to trade off accuracy in the linear dispersion relation for accuracy in kinematics in choosing the expansion depth.

Since the Boussinesq family of models is based on the assumptions that nonlinearity and dispersion are both weak and of comparable magnitude, it is of interest to examine the validity of these assumptions across the shoaling zone. We define the maximum nonlinearity and dispersion using local measures as:

$$\epsilon \equiv \frac{u}{c} \tag{21}$$

and

$$\mu^2 \equiv (kh)^2 \equiv \left(\frac{u_{xx}}{u}\right) h^2 \tag{22}$$

where u_{xx} is evaluated as u_{zz} as discussed previously, and all values are evaluated under the wave crest.

The evolution of the nonlinear parameter, ϵ, and the dispersion parameter, μ^2, across-ing the shoaling zone are presented in Figure 11. The relative importance of these two

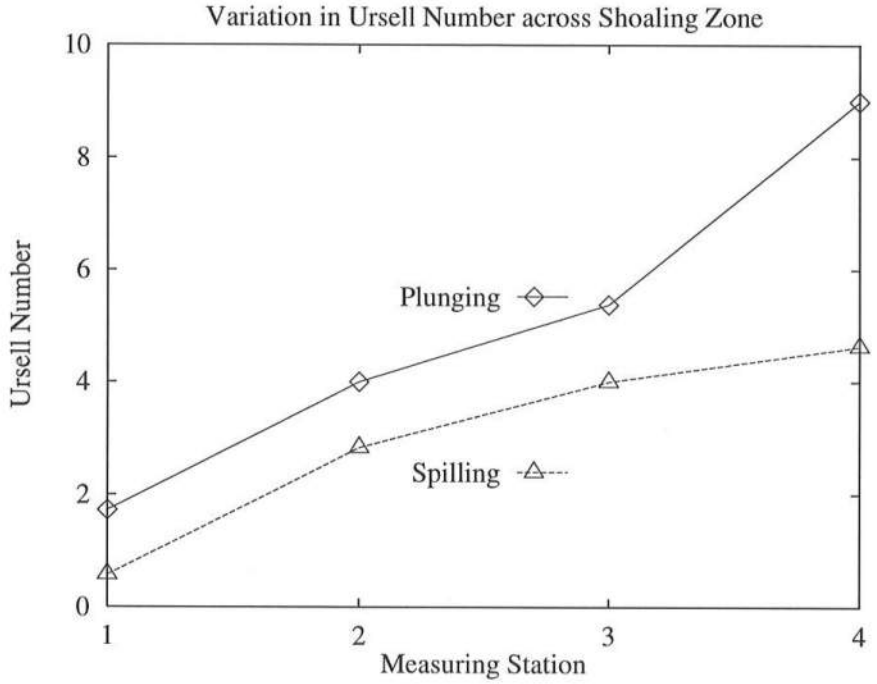

Figure 12: Ratio of the nonlinearity (ϵ) to the dispersion (μ^2) as a function of position in the shoaling zone for the 2 s (spilling) and 5 s (plunging) waves. All values are defined under the wave crest.

perturbations to the shallow water equations changes significantly as the wave shoals. The Ursell number (ϵ/μ^2) is shown for the two wave cases in Figure 12. Both the spilling and plunging wave cases are characterized by greater dispersion than nonlinearity in the flat-bottom region (station 1). As the wave shoals, this ordering is reversed in both cases, with a strong dominance of nonlinearity in both cases. The wave breaks within 0.40 m (1/10 of a wavelength) of the last station, so these results capture most of the pre-breaking wave transformations.

5 Summary

For the important test case of shoaling regular (cnoidal) waves, we have shown that (1) the local kinematic balance determining the vertical structure of horizontal velocity is best described by the Boussinesq models optimized for the linear dispersion relation; and (2) this result is not modified by the significant increase in nonlinearity as the wave shoals.

Based on local definitions of the dispersive and nonlinear parameters, we see that the assumption of weak dispersiveness in the Boussinesq model actually improves slightly across the shoaling zone, while the assumption of weak nonlinearity becomes less accurate.

These observations suggest that improvements in the treatment of the nonlinear terms (such as the fully nonlinear Boussinesq model of [6]) are more important than further improvements in the treatment of dispersive terms in this region.

Although these results do not negate the known weaknesses of Boussinesq models in modelling strongly shoaling waves, they do show that the general philosophy of optimizing the linear dispersion relation is a reasonable and effective one for regular shoaling waves.

6 Acknowledgments

This research was supported by a University Research Initiative Grant from the Army Research Office of the Department of Defense, contract number DAAL 03-92-G-0116.

References

[1] D. G. Goring. *The Propagation of Long Waves onto a Shelf.* PhD thesis, California Institute of Technology, 1978.

[2] O.S. Madsen and C.C. Mei. The transformation of a solitary wave over an uneven bottom. *J. Fluid Mech.*, 39:781–791, 1969.

[3] A. D. McCowan. The range of Boussinesq type numerical short wave models. In *Proc. 22nd IAHR Congr.*, 1987.

[4] O. Nwogu. An alternative form of the Boussinesq equations for nearshore wave propagation. *J. Wtwy., Port, Coast. and Ocean Engineering*, 119:618–638, 1993.

[5] D. H. Peregrine. Long waves on a beach. *J. Fluid Mech.*, 27(4):815–827, 1967.

[6] Ge Wei and James T. Kirby. A fully nonlinear Boussinesq model for surface waves. I. highly nonlinear, unsteady waves. *J. Fluid Mech.*, 1995. In press.